

Criteria for Selection of Target-Materials and Design of High-Efficiency-Release Targets for Radioactive Ion Beam Generation

G. D. Alton,¹ J. R. Beene, and Y. Liu

Physics Division, Oak Ridge National Laboratory,² P. O. Box 2008, Oak Ridge, TN 37831-6368

Abstract

In this report, we define criteria for choosing target-materials and for designing, mechanically-stable, short-diffusion-length, highly-permeable targets for generation of high intensity radioactive ion beams (RIBs) for use at nuclear physics and astrophysics research facilities based on the ISOL principle. In addition, lists of refractory target-materials are provided and examples are given of a number of successful targets, based on these criteria, that have been fabricated and tested for use at the Holifield Radioactive Ion Beam Facility (HRIBF).

Keywords: actinide, carbon - C, characterization of target, cooling of target, CVD, electrodeposition, electrophoresis, fiber target, foam target, heating of target, heavy ion target, ion implantation, ion source, isotope separation, liquid target, multi-layer target, pellet target, protective layer, radioactive beam, radioactive target, target list, vacuum deposition, very thin target

¹ Corresponding author: FAX: 423-574-1268, e-mail: gda@ornl.gov.

² Managed by Lockheed Martin Energy Research Corp. under contract DE-AC05-96OR22464 with the U.S. Department of Energy.

1. Introduction

Many of the reactions fundamentally important in nuclear physics and astrophysics are inaccessible to experimental study using stable-beam/stable-target combinations and therefore can only be studied with accelerated radioactive ion beams (RIBs). The availability of RIBs offers unique opportunities to further our knowledge about the structure of the nucleus, the stellar processes that power the universe and the processes responsible for heavy element formation. As a consequence of the world-wide interest in the potential benefits of using RIBs for such research, facilities have been built, funded for construction or proposed for construction in Asia, Europe and North America; these include the Holifield Radioactive Ion Beam Facility (HRIBF) at the Oak Ridge National Laboratory (ORNL) [1]. Many of the facilities are based on the well-known Isotope Separator On-Line (ISOL) in which radioactive nuclei are produced by fusion-evaporation, spallation, or fission nuclear reactions induced by high-energy proton, deuteron, *He*, heavy-ion beams or neutron beams. These facilities differ primarily in the ion beams used for production of the radioactive species (e.g., *p*, *d*, ^3He or ^4He , etc.) and the type (cyclotron, synchrotron, or linear accelerator) and maximum energy capability of the light-ion, production accelerator. (Production beam energies at existing ISOL facilities range between 30 and 1000 MeV.)

Important experiments have been done with radioactive beams of 100 particles/s or less, however, broad successful programs in nuclear structure physics or nuclear astrophysics research will require much higher radioactive ion beam (RIB) intensities ranging up to intensities now used in stable-beam experiments. Maximum production rates are set by the reaction cross sections for producing the species of interest and the practical limits of the primary beam intensity, in terms of maximum permissible power-density-on-target that can be used without compromising the efficiency of the ion source or the physical integrity of the target. Since the production rates and number of radioisotopes (or nuclides) produced increase significantly with primary beam energy, high-energy primary beams are also highly desirable. Delay times due to diffusion-release from the target-material and effusive-flow of the radioactive species to the ion source are the principal RIB intensity limiting processes. Experimentally useful RIBs of very short-lived species are often difficult to generate, since they must be diffused from the interior of the target-material, effusively transported to the ionization chamber of the source, ionized, extracted, mass analyzed, and accelerated to research energies in a time-span commensurate with their lifetimes. The speeds at which these processes must take place, impose stringent requirements on the selection of appropriate high-temperature, refractory target-materials, the design of fast-release targets and vapor-transport systems, and the choice of high-efficiency ion sources for RIB generation.

The ISOL/injection high-voltage platform system used at the Holifield Radioactive Ion Beam Facility (HRIBF) for production, generation, isotope-separation, and injection of radioactive ion beams into the 25-MV Tandem post accelerator is illustrated schematically in Fig. 1. Since the 25-MV Tandem accelerator is a negative-ion accelerator, it is necessary to convert initially positive ions beams to negative polarity prior to injection. An isometric drawing of a target/ion source used at the HRIBF is shown in Fig. 2, illustrating the position of the target and point of entry of the production beam into the target-material relative to the ionization chamber of the source. As noted, the target is close-coupled to the ion source to minimize transport-time between diffusion release from the target-material and the ionization chamber of the source. Figure 3 shows a cross-sectional view of a prototype target/heat-sink system that houses the target-material; the system is designed to remove a fraction of the beam-deposited heat from the target-material and thereby permit an increase in the production beam intensity.

2. Processes that affect RIB intensities

The principal means whereby short half-life radioactive species are lost between initial formation and utilization are associated with the times required to diffuse the species of interest from

the target-material and to transport them to the ionization chamber of the source in relation to their lifetimes. The diffusion (solid-state) and surface adsorption/desorption processes depend exponentially on the operational temperature of the target/ion source. Therefore, it is incumbent to choose highly refractory, target-materials so that the transport system can be operated at high temperatures to minimize delay times associated with these processes. The diffusion and surface adsorption processes are briefly described below.

2.1 Diffusion

Nuclear reaction product species, embedded in a chemically dissimilar target-material, are released from the material through a binary diffusion mechanism. Impurity atoms or vacancies will move through the solid until equilibrium is reached. The rate at which the diffusion process takes place depends exponentially on the temperature for solid diffusion-couples. The net flux, J , of either atoms or vacancies is related to the gradient of concentration, ∇n , by Fick's first equation given by:

$$J = -D\nabla n \quad (1)$$

where D is the diffusion coefficient. Knowledge of D is required to estimate the release rates of particular species. In general, D must be measured by techniques such as described in Refs. 2 and 3 or by ion implantation methods developed for this purpose [4-6]. Fortunately, large sets of data for certain diffusion-couples are available from resources such as cited in Refs. 7-9. The ion implantation technique, employed at the HRIBF, is particularly useful for measuring diffusion coefficients for candidate species/target-material combinations [5,6].

The time-dependent form of Eq. 1 is known as Fick's second equation. The three-dimensional form of this equation, which allows for creation of particles $S(x,y,z,t)$ as well as loss of particles $E(x,y,z,t)$, can be expressed in a Cartesian coordinate representation as follows:

$$\frac{\partial n}{\partial t} = D \left(\frac{\partial^2 n}{\partial x^2} + \frac{\partial^2 n}{\partial y^2} + \frac{\partial^2 n}{\partial z^2} \right) + S(x,y,z,t) - E(x,y,z,t) \quad (2)$$

where D is assumed to be independent of concentration. Planar, cylindrical, and spherical geometry targets will be used or are envisioned for use at the HRIBF.

Solutions to the respective time dependent form of Eq. 2, appropriate for the particular target-material geometry, can be found either by separation of variables, the use of Laplace or Fourier transformation techniques, or by standard numerical computational techniques or in combination. We assume that the cross-section is independent of production beam energy resulting in a uniform distribution of species in the path of the beam. For the more general case, the distribution function S must be chosen to represent the actual distribution of the radioactive species within the target-material. For a uniform distribution of particles such as assumed in the production of radioactive species with a primary ion beam of intensity I particles per second, the production rate density S is given by

$$S(x,t) = \sigma N_T IL / V \quad (3)$$

N_T is the number of target nuclei per unit volume; L is the length of the target material; σ is the cross-section for production of the species of interest; and V is the volume of the beam-target overlap region.

For production of radioactive species with half-life $\tau_{1/2}$, E is given by

$$E(x,t) = n\lambda \text{ where } \lambda = 0.693/\tau_{1/2} \quad (4)$$

where n is the concentration of radio-nuclei in the target material.

Solid-state diffusion. For solid-state diffusion, the diffusion coefficient is dependent on the activation energy H_A required to move the atoms or vacancies from site to site, and on the temperature T of the solid, according to:

$$D = D_0 \exp(-H_A/kT) \quad (5)$$

where k is Boltzmann's constant and D_0 is a constant. D is related to the vibration frequency and lattice parameters of the particular atom/crystal couple. Typical values for this process range between 10^{-16} m²/s and 10^{-12} m²/s for target temperatures in the range of 1873-2073 K. H_A can be extricated from experimental data by measuring the target temperature dependence of D on T with methods such as described in Refs. 2 and 3 or by the use of ion implantation [4-6].

Liquid-state diffusion. In contrast to the case of diffusion within a solid target, the diffusion coefficient for particles in liquid targets is weakly dependent on the temperature according to

$$D \approx \alpha d [\sqrt{8k/\pi M}] T^{3/2} \quad (6)$$

where α is the coefficient of thermal expansion of the liquid target-material, d is the diameter and M the mass of the solute atom. D has typical values of a few times 10^{-9} m²/s. Because of the fact that the process is only weakly dependent on the temperature T , there is no particular gain achieved by heating the material significantly above its melting point other than through reducing surface desorption times as will be discussed later. As noted, diffusion coefficients for liquids are several orders of magnitude larger than those for their solid-state counterparts and therefore are especially attractive for short-lived species; unfortunately, few elemental metals have the vapor pressure characteristics commensurate with these applications. To take advantage of the fast diffusion properties of liquid-state targets, eutectic alloys can be employed as a means of reducing the melting points of refractory metals.

2.2 Vapor Transport

Time delays, associated with adsorption, which are excessively long in relation to the lifetime of the radioactive species, can result in significant losses of beam intensity in an ISOL facility. The residence time of a particle on a surface is given by the Frenkel equation:

$$\tau = \tau_0 \exp[-H_{ad}/kT] \quad (7)$$

where H_{ad} is the heat of adsorption or enthalpy required to evaporate the atom or molecule from the surface, k is Boltzmann's constant, T is the absolute temperature, and τ_0 is the time required for a single lattice vibration ($\sim 10^{-13} - 10^{-15}$ s). The heat of adsorption increases with increasing chemistry between the adsorbed atom and the surface where the adsorption takes place. This value varies widely depending upon the adsorbent/adsorbate combination.

The desorption rate of atoms per unit area dN'/dt in thermal equilibrium with a surface at temperature T is given by

$$\frac{dN'}{dt} = \frac{P(T)N'kT}{h} \exp\left[\frac{(\Delta S T - H_{ad})}{kT}\right] \quad (8)$$

where $P(T)$ is the temperature-dependent probability that the particle will stick to the surface (sticking coefficient), N' is the number of atoms adsorbed per unit area, h is Planck's constant; ΔS is the change in entropy of the adsorbed particle; and H_{ad} is the heat of adsorption [10].

Since it is desirable to minimize the residence times of atoms/molecules on surfaces in the target/ion source, the choice of the materials of construction for the vapor transport system of the source is extremely important. (For example, the time required for transport of a particular species can be reduced by selectively choosing the materials of construction for the vapor transport system or coating surfaces such as *Ta* with low enthalpy of adsorption materials such as *Re* [11].) This choice should be made after careful analyses of the time required for transport of the species of interest through the various available refractory materials that are options for constructing the vapor transport system. For example, selection of the appropriate material from which to construct the vapor-transport-system for fast and efficient transport of a particular radioactive species can be made on a time-dependent basis by use of Monte Carlo simulation techniques or analytical expressions which include adsorption/desorption processes. The following time dependent expression for the number of particles N in a tubular volume of length l and radius a after time t has been found particularly useful for this purpose [12]:

$$N = N_0 \exp\{-t/\tau\} \quad (9)$$

where N_0 is the number of particles in the volume at time $t = 0$. In Eq. 9, τ is given by

$$\tau = 3/4 \left[N_b \tau_0 \exp\{-H_a/kT\} + L/v \right] \quad (10)$$

where N_b is the average number of bounces that the particle makes during passage through the tube; τ_0 is the time for a single lattice vibration ($\sim 10^{-13} - 10^{-15}$ s); H_a is the enthalpy of adsorption; L is the average distance a particle travels during passage through the tube and v is the velocity of the particle of mass M . Figs. 4 and 5 display, respectively, distribution functions for *As*, effusively transported in either *Ta* and *Ir* or *Re* tubes from the target reservoir to the ionization chamber of the electron-beam-plasma ion source (EBPIS) used at the HRIBF [13], as calculated by use of the Monte Carlo code *Effuse* [14] and with Eq. 9. *Re* is clearly the better choice for short-lived species. The enthalpies of adsorption were taken from Ref. 15.

3. Target-material Selection Criteria

3.1 Limiting Target Temperature Selection Criterion

Target-material selection begins by considering the physical, chemical, and thermal properties of the target-material in relation to those of the product species. One of the principal problems lies in the availability of target-materials that are sufficiently refractory so that they can be raised to the temperatures necessary for fast release of the product species without excessive vaporization/sublimation of the target-material itself. The choice of material is further restricted by the requirement that the radioactive species be easily diffused from the target-material and readily volatilized for subsequent transport to the ionization region of the source. Thus, in the ideal case, the radioactive species should possess physical and chemical properties almost opposite to those of the target-material itself. For example, the species should not form refractory compounds within the

target-material, rapidly diffuse to the surface, either in elemental or compound form, and upon reaching the surface, be readily desorbed. These idealized differences in chemical and physical properties of the target/species combination are not often realizable, particularly for close lying elements where their physical and chemical properties are often similar.

Since the diffusion coefficient D in a solid depends exponentially on the operational temperature of the target, it is desirable to heat the target to temperatures as high as practical. The upper limit to which any target can be operated depends on the vapor pressure of the target-material or composite target in relation to the sensitivity of the ionization process to particle density within the ionization volume of the source. Thus, the *limiting temperature* of the target-material is defined as the temperature at which the vapor pressure begins to deleteriously affect the ionization efficiency of the particular ion source used in the RIB generation process. Therefore, it is most essential to know the upper temperature limit to which the target material can be raised; this value serves as one of the most important criteria for selecting a particular target-material. For example, the limiting vapor pressure is $\sim 2.67 \times 10^{-2}$ Pa for the EBPIIS used at the HRIBF [13]. (This criterion has been experimentally verified for several successful targets at the HRIBF.) However, the choice of high-limiting temperature material alone does not guarantee fast, nor efficient, release of the species of interest from the target. It is imperative that the product species diffuse from the target-material within its lifetime and thus, the diffusion coefficient must be known or experimental release studies made for the particular target/species combination before reaching a definitive conclusion in the selection process.

As classic examples of close-to-ideal target/radioactive species combinations, we cite cases such as the production of ^{13}N through the $^{12}\text{C}(d,n)^{13}\text{N}$ reaction to form the gaseous $^{12}\text{C}^{13}\text{N}$ molecule or for the production of $^{14,15}\text{O}$ through the respective reactions $^{12}\text{C}(^3\text{He},n)^{14}\text{O}$ and $^{12}\text{C}(^4\text{He},n)^{15}\text{O}$ to form the gaseous and pseudo-noble $^{12}\text{C}^{14,15}\text{O}$ molecule. Analogously, ^{30}S can be formed in SiC or SiO_2 through the respective reactions, $^{28}\text{SiC}(^3\text{He},n)\text{C}^{30}\text{S}$ and $^{28}\text{SiO}_2(^3\text{He},n)^{30}\text{SO}_2$ where the release products, C^{30}S and $^{30}\text{SO}_2$, are both gaseous over a wide range of temperatures. As an illustration of how the selection process is effected, we take SiC as an example. The vapor pressure versus temperature for SiC is shown in Fig. 6, while Figs. 7 and 8, respectively, display thermal-equilibrium compositions of the target-material, SiC , and the product species, CS versus temperature. From such analyses, the temperature limit of the target-material and thermal stability of the release product can be assessed. Of the two target options for producing and releasing ^{30}S (i.e., SiC or SiO_2), SiC is the better choice since it can be operated up to 1933 K while SiO_2 can only be operated up to 1773 K. In addition, the release product CS is almost chemically inert and is thermally stable over the complete operational range of the ion source, whereas SO_2 is very chemically active and begins to decompose at ~ 1773 K.

Further examples of the use of the vapor-pressure criterion for selecting target-materials with high upper-limit operating temperatures are displayed in Fig. 9; Al_2O_3 , Y_2O_3 , ZrO_2 and HfO_2 compounds have either been used at the HRIBF or are candidates for use in generating RIBs of $^{17,18}\text{F}$. Thermal equilibrium compositions of Al_2O_3 , ZrO_2 and HfO_2 versus temperature are shown, respectively, in Figs. 10-12; please note that the temperatures at which these compounds begin to dissociate complement those derived from vapor pressure data, displayed in Fig. 9, for the EBPIIS [13] with a limiting operational pressure of 2.67×10^{-2} Pa. Fibrous targets of these materials, in combination with the new kinetic ejection negative ion source [16], have been successfully employed at the HRIBF for the efficient release of the isotopes of F^- [17-19]. Further examples of the use of the vapor pressure criterion in the selection of UC_2 and ThC_2 target-materials for production of neutron-rich radio-nuclei are shown in Fig. 13. Their complementary thermal-equilibrium compositions versus temperature are shown, respectively, in Figs. 14 and 15. Obviously, ThC_2 would be a better choice since it has a higher limiting temperature.

3.2 Other Target-Material Selection Considerations

Obviously, target-materials with the highest percentage of the production nuclei are desirable in order to maximize the production rate of the species of interest. Still other factors complicate the choice of target-material, such as the presence of high atomic number nuclei that do not contribute to the production of the species of interest, but slow the production projectile down at a faster rate and, thereby, generate more heat in the target than necessary because of their larger dE/dx (stopping powers). For example, in choosing a particular target-material for an application in which the production element is common in a group of refractory compounds such as O for the production of F isotopes with Al_2O_3 , Y_2O_3 , ZrO_2 or HfO_2 , one must take into consideration increases in dE/dx with atomic number Z , and the higher consequent target-temperatures for a given production-beam intensity due to increases in beam-deposited heat. Heavy nuclei may also produce unwanted, long-lived radioactive by-product species that complicate the radioactive material-handling problem.

3.3 Target-materials

Table 1 provides examples of several candidate target-materials for production of proton-rich nuclei through fusion-evaporation and fission reactions at a low energy primary beam RIB facility, such as the HRIBF; analogously, candidate target-materials for the production of proton-rich and neutron-rich radioactive species through spallation or fission reactions, produced with 1-GeV protons, are listed in Table 2. A broad range of neutron-rich nuclei can be produced in fission targets such as UC_2 and ThC_2 for the low-energy HRIBF as well as for high-energy facilities. Although the product species listed for a given target-material in Tables 1 and 2 can be produced through the respective nuclear reactions, many of these targets have not yet been tested on-line and not all of the species can be efficiently diffused from the particular target-material because of unfavorable physical and chemical properties of particular species/target-material combinations. The list of reactions and target materials is not comprehensive nor is it intended to suggest that a particular production reaction/target material combination is the best combination for production and release of a given species. In cases where the species of interest cannot be released from the target matrix, due to strong chemical reactions alternative target-materials must be considered. Since the species of interest must be expeditiously released from the volume of the target-material within its lifetime through the sensitive temperature dependent diffusion mechanism, all other parameters being equal, target-materials with the highest limiting temperatures are the most desirable.

4.0 Target Design and Fabrication

Efforts are presently being directed toward the design and fabrication of new concept targets with the short diffusion lengths, high-permeability properties, and controllable temperatures required for meeting the RIB intensity needs for a wide-range of species for nuclear and astrophysics research at ISOL-based facilities, including the HRIBF. These new concepts include the use of low-density target matrices, such as carbon-bonded-carbon-fiber (CBCF) or reticulated-vitreous-carbon-fiber (RVCF), to serve as the thermal conduit for transport of heat deposited in the matrix by the production beam to a properly designed heat-sink and as the plating matrix for the target-material itself. Since short-lived particles must swiftly diffuse from the target-material, the diffusion lengths must be short (thin target-materials) and the target temperature must be as high as practicable.

4.1 Target Dimensional Design Criteria

The form of the diffusion equation (Eq. 2) can be solved for the appropriate target geometry (planar, cylindrical, or spherical) to derive simple, analytic expressions that relate the dimensions of the target-material with the diffusion time τ that will release ~70% of the species of interest within its lifetime, provided that the diffusion coefficient is known at the operating temperature of the target-

material. Expressions for optimizing the target thickness of planar, cylindrical, and spherical geometry targets are given below:

A plate of thickness, x :

$$x(cm) = \pi\{D\tau\}^{1/2} \quad (11)$$

A rod of diameter, d_r :

$$d_r(cm) \cong 4.8\{D\tau\}^{1/2} \quad (12)$$

A sphere of diameter, d_s :

$$d_s = 2\pi\{D\tau\}^{1/2} \quad (13)$$

Thus, by engineering target-material dimensions according to these basic relations, one can optimize the release rate of a particular radioactive species. Table 3 provides information for targets of optimum thickness for the release of selectively chosen radioactive species. The respective release rates of ^{17}F from a target-material such ZrO_2 , cast in each of the three principal geometries with common dimensions in the direction of diffusion, are illustrated in Fig. 16. This philosophy has been followed in designing highly permeable fibrous- and composite-targets as well as liquid-metal target concepts for use in the HRIBF research programs as described below:

4.2 Target Matrices

Carbon matrices. Since only a few materials can be procured in fibrous form, it is desirable to find universal, low-density, highly permeable matrices for their deposition. Their thicknesses are determined by the prescriptions dictated by use of Eqs. 11, 12, or 13, depending on the target-material geometry for maximizing the diffusion-release of species in question when operated at the limiting temperature of the target-material. Furthermore, it is desirable that the matrix have good thermal conductivity attributes so that the beam-deposited heat can be removed at a controlled rate with properly designed heat-sink system so that, in combination, the target matrix can be operated at the maximum allowable primary beam intensity as dictated by the temperature limitation. Carbon-bonded-carbon fibers (CBCF) and reticulated-vitreous-carbon fibers (RVCF) offer highly permeable, machinable, matrices for deposition of generic target-materials onto their surfaces. Still other as yet untested materials, such a pitch-derived-carbon-foam (PDCF), are candidates for this application [20]. CBCF ($\rho \sim 10\% \rho_0$) is made of cylindrical fibers sintered together at the points of intersection, while RVCF ($\rho \sim 2\% \rho_0$) and PDCF ($\rho \sim 10\% \rho_0$) are continuous ligament structures. RVCF has a tetrakai-decahedral structure while PDCF is a spherical-void structure. These materials can be machined to the geometry desired for the particular target application prior to depositing the specified thickness of target-material onto the surface. In cases where the target-material and the matrix will chemically react at elevated temperatures to form volatile compounds, the matrix must be pre-coated with a protective material such as *Ta*, *W*, *Ir* or *Re* to prevent the undesired reaction process. *Re* is particularly appealing for this application because of its low adsorption-enthalpy properties for electro-negative elements/molecules. These matrices can also be CVD/CVI (chemical-vapor-deposition/chemical-vapor-infiltration) coated with refractory metals such as *Zr*, *Nb*, *Mo*, *Hf*, *Ta*, *W* and *Re* to form composite targets for producing proton-rich radio-nuclei for use at high-energy ISOL facilities.

Metal-foam matrices. Methods have been developed for producing low-density ($\rho \sim 5-10\% \rho_0$) metal foams that have potential use as stand-alone targets or as matrices for wicking liquid-metals into the path of the production beam. The latter concept is particularly appealing for production of short-lived

species because of the enhanced diffusion rates from liquid-phase targets. Fig. 17 displays a SEM of *Rh* metal foam ($\rho \sim 8\% \rho_0$).

4.3 Coating Methods

Techniques are presently available that can be used to uniformly deposit specified thicknesses of the material in question onto the support matrix of choice. At this point in time, several target coating schemes are being used or are under consideration for use for this purpose, they include: chemical vapor deposition (CVD); chemical vapor infiltration (CVI); chemical reaction deposition (CRD); physical vapor deposition (PVD); electrolytic deposition (ED), cathophoresis deposition (CD), electrophoresis deposition (ED) and sol-gel coating (SGC).

5.0 Targets

5.1 Fibrous Targets

In a few cases, fibrous materials with small diameters are available. These materials include Al_2O_3 , SiO_2 , Sc_2O_3 , TiO_2 , Y_2O_3 , ZrO_2 , HfO_2 , Ta_2O_5 and rare-earth oxides. Figures 18 and 19, respectively, display examples of Scanning Electron Micrographs (SEMs) of small diameter SiO_2 and HfO_2 fibrous materials that are candidates for the production of certain proton-rich species. Al_2O_3 , ZrO_2 and HfO_2 fibrous materials have been successfully used to produce and efficiently release $^{17,18}F$ for use or potential use in the HRIBF astrophysics research program [17-19]. All of these candidate target-materials have thin fiber diameters and are highly permeable as required for high release efficiency.

5.2 Composite Targets

The examples of highly permeable targets that were fabricated by use of one of the coating processes described previously are shown, respectively, in Figs. 20-23. A scanning electron micrograph (SEM) of a CBCF matrix CVD coated with $\sim 5 \mu m$ of SiC for potential use at the HRIBF for the generation of certain isotopes of *S* and *P* is shown in Fig. 20. Figure 21 displays a SEM of a RVCF matrix electroplated with a thin layer ($2 \mu m$) of *Ni* metal for potential use at the HRIBF for the generation of ^{58}Cu . This target has been used on-line in low-intensity experiments and found to efficiently release short-lived isotopes of *Cu* [21]. In particular, the CVD process can be used to fabricate uniform deposits of a variety of refractory metals as well as other materials for potential use for the spallation production of proton-rich nuclei with high-energy proton beams, as suggested in Table 2. As an example of such composite refractory metal targets, a SEM of CVD of *W* on RVCF is displayed in Fig. 22. Chemical-reaction deposition (CRD) technique is also a viable option for the formation of thin-layer targets of certain materials. Fig. 23 displays a SEM of UC_2 deposited by this technique for the production of neutron-rich species for RIB applications. The UC_2 target has been tested on-line and found to efficiently release a wide spectrum of short-lived species [22].

5.3 Liquid-Metal Targets

Prototype liquid-metal targets have been successfully used for the production and release of ^{58}Cu ($\tau_{1/2}=3.2s$) from liquid *Ni* and analogously, for the production and release of ^{69}As ($\tau_{1/2}=912 s$) from liquid *Ge* at the HRIBF [21]. If we assume that $D = 3 \times 10^{-9} m^2/s$ for ^{58}Cu in liquid *Ni* and $D = 5 \times 10^{-9} m^2/s$ for ^{69}As in liquid *Ge*, then optimum target thicknesses x for planar-geometry liquid-targets, that will release 70% of the species within their respective half-lives, can be calculated

from the expression for the diffusion length given by Eq. 11 ($x = \pi\sqrt{D\tau_{1/2}/2}$), assuming that targets for these isotopes have an impermeable boundary at the interface between the receptacle and the liquid-metal. The respective values for these two isotopes are $x = \sim 154 \mu\text{m}$ for $^{58}\text{Cu/Ni}$ and $x \sim 3350 \mu\text{m}$ for $^{69}\text{As/Ge}$. Fig. 24 illustrates a scenario in which the HRIBF production beam is incident at a shallow angle with respect to the plane of a horizontally mounted liquid-metal target-material; the angle is chosen so that both optimum production and fast diffusion release can occur simultaneously. The use of liquid-metal alloy targets significantly increases the number of candidate liquid-metal target-materials. Table 4 provides a listing of such materials and optimum thicknesses for the release of selected radio-nuclei.

6.0 Target/Heat-Sink Systems

The target/heat-sink assembly design must be optimized so that the particular target composite matrix can be maintained at a prescribed temperature which is limited by the maximum vapor pressure of the target-material that can be tolerated before compromising the ion source efficiency and/or destroying the target through sublimation/vaporization processes. Since the target-material is heated by energy deposited in the target-material by the primary (production) beam, it is imperative that some fraction of this heat be removed by some means so that as high as practical primary ion beam can be utilized and so that the total target envelope can be heated independently and controlled at the desirable temperature. This is a serious problem that has not been satisfactorily solved to-date for a wide variety of primary beam intensities, targets, and target-materials. However, we are presently devoting considerable effort to this problem for the present HRIBF facility. An example of a target/heat-sink system design, as yet untested, for removing beam-deposited heat from highly permeable Al_2O_3 fibrous target during on-line operation of the HRIBF is illustrated in Fig. 25. Target/heat-sink systems are designed by use of the finite analyses programs such as ANSYS [23].

Acknowledgements

The authors are especially indebted to members of the HRIBF Facility Operations Group for on-line evaluation of the diffusion release properties of various fibrous and liquid targets and to R. Gard for providing LAHET-derived [24] species and yield information for the spallation and fission target-materials listed in Table 2.

References

- [1] R. Auble, *Proceedings of the Applications of Accelerators in Research and Industry*, eds. J. L. Duggan and I. L. Morgan, AIP Press, New York, CP475 (1999) p. 292; G. D. Alton and J. R. Beene, *J. Phys. G: Nucl. Part. Phys.* **24** (1998) 1347.
- [2] P. Shewmon, *Diffusion in Solids*, A publication of the Minerals, Metals and Materials Society, Second edition, 1989.
- [3] R. Kirkaldy and D. J. Young, *Diffusion in the Condensed State*, the Institute of Metals, London, 1987.
- [4] R. Kirchner, *Nucl. Instr. and Meth. B* **70**, (1992) 186.
- [5] G. D. Alton, J. Dellwo, H. K. Carter, I. Y. Lee, C. M. Jones, J. Kormicki, G. diBartolo, J. C. Batchelder, J. Breitenbach, J. A. Chediak, K. Jentoff-Nilsen and S. Ichikawa, *Proc. Int. Conf. on Neutrons and their Applications*, eds. G. Vourvopoulos and T. Paradellis, SPIE, Vol. 2329 (1994) p. 335.
- [6] G. D. Alton and J. Dellwo, *Nucl. Instr. and Meth. A* **382**, (1996) 225.
- [7] *Numerical Data and Functional Relationships in Science and Technology-New Series, Group-3*, founded by H. Landolt and R. Börnstein, ed., W. Martienssen: *Condensed Matter*, Vol. 26; *Diffusion in Solid Metals and Alloys*, Springer-Verlag Berlin, (1998).
- [8] A. K. Roy and R. P. Chhabra, "Diffusivities in of Metallic Solutes in Molten Metals," in *The Handbook of Chemistry and Physics*, 76th edition, Ed.-in-Chief, D. R. Lide, CRC Press, Boca Raton, (1995-1996) Ch. 6, p. 258.
- [9] DICTRA is a database diffusion code that is a product of the Royal Institute of Technology, Stockholm, Sweden.
- [10] S. D. Kevan, *Proc. of the Appl. of Accel. in Research and Industry*, eds., J. L. Duggan and I. L. Morgan, CP392, AIP Press, New York, p. 425.
- [11] G. D. Alton, J. Dellwo, H. K. Carter, I. Y. Lee, C. M. Jones, J. Kormicki, and D. K. Olsen, *Nucl. Instr. and Meth. B* **66**, (1992) 492.
- [12] Analytical formula, developed by G. D. Alton and J. C. Bilheux, for estimating effusive-flow through tubular vapor transport systems.
- [13] G. D. Alton, *Nucl. Instr. and Meth. A* **382** (1996) 207; G. D. Alton, D. L. Haynes, G. D. Mills, and D. K. Olsen, *Nucl. Instr. and Meth. A* **328**, (1993) 325.
- [14] *Effuse* is a Monte Carlo computer code written by J. Dellwo and G. D. Alton for estimating effusive-flow through tubular vapor transport systems.
- [15] H. Roßbach and B. Eichler, Zentralinstitut für Kernforschung, Rossendorf, Report ZfK-527 (1984).
- [16] G. D. Alton, Y. Liu, C. Williams, and S. N. Murray, *Proceedings of Eighth International Conference on Heavy Ion Accelerator Technology*, CP473, ed. K. W. Shepard, AIP Press, New York, p. 330.
- [17] G. D. Alton, *Proceedings of the Application of Accelerators in Research and Industry*, editors, J. L. Duggan and I. L. Morgan, CP392, AIP Press, New York, p. 429.
- [18] D. W. Stracener, H. K. Carter, J. B. Breitenbach, J. Kormicki, J. C. Blackmon, M. S. Smith and D. W. Bardayan, *Proceedings of the Application of Accelerators in Research and Industry*, editors, J. L. Duggan and I. L. Morgan, CP392, AIP Press, New York, p. 392.
- [19] D. W. Bardayan et. al, *Phys. Rev. Lett.* **83** (1999) p. 45.
- [20] J. Klett, *Proc. Int. SAMPE Symposium, May 31-June 4, 1998*, Anaheim, CA, SAMPE, p. 745.
- [21] D. W. Stracener et al. (unpublished).
- [22] G. D. Alton and D. W. Stracener (unpublished).
- [23] ANSYS is a finite element code designed to simulate thermal transport, mechanical stress and electromagnetic problems; the code is marketed by ANSYS, Inc., Houston, PA.
- [24] *The LAHET Code System*, LA-UR-89-3014, R. Prael and H. Lichtenstein, Los Alamos National Laboratory, September 1989.

Figure Captions

Fig. 1. ORNL 93-12227. A schematic illustration of the ISOL/high-voltage platform injection system used for production, negative-ion beam generation, isotope separation and injection into the 25-MV Tandem electrostatic accelerator used to accelerate RIBs to research energies at the Holifield Radioactive Ion Beam Facility (HRIBF) [1].

Fig. 2. ORNL 99-0429_b. An isometric of the target/ion source arrangement used at the HRIBF for radioactive ion beam (RIB) generation. The ion source is an electron beam plasma ion source (EBPIS) patterned after the CERN-ISOLDE design [13].

Fig. 3. ORNL 99-04252. Cross sectional view of a target/heat-sink system designed for production and fast release of fission product radioactive species.

Fig 4. Simulation of *As* effusively transported in a *Ta* tube from the target reservoir to the ionization chamber of the EBPIS source used at the HRIBF [13] as calculated with the Monte Carlo code *Effuse* [14] and by use of the analytical expression, Eq. 9.

Fig 5. Simulation of *As* effusively transported in a *Re* tube from the target reservoir to the ionization chamber of the EBPIS source used at the HRIBF [13] as calculated with the Monte Carlo code *Effuse* [14] and by use of the analytical expression, Eq. 9.

Fig 6. Vapor pressure of *SiC*. *SiC* is a candidate target-material for producing ^{30}S and ^{30}P . The target-material can be operated up to the limiting temperature set by the vapor pressure of the particular ion source above which the ionization efficiency of the source is deleteriously affected. This temperature is $\sim 2.67 \times 10^{-2}$ Pa for the EBPIS used at the HRIBF [13].

Fig. 7. ORNL 99-04280A. Thermal equilibrium composition of *SiC* as a function of temperature. *SiC* is a candidate target-material for the production ^{30}S through the reaction $^{28}\text{SiC}(^3\text{He}, n)^{30}\text{SC}$.

Fig. 8. ORNL 99-04281A. Thermal equilibrium composition of *CS* as a function of temperature. *CS* is the gaseous diffusion release carrier of ^{30}S formed through the reaction $^{28}\text{SiC}(^3\text{He}, n)^{30}\text{S}$.

Fig. 9. Vapor pressure versus temperature for Al_2O_3 , Y_2O_3 , ZrO_2 and HfO_2 . These targets are candidates for the generation of several proton-rich, radio nuclei and can be operated up to the limiting temperatures set by the vapor pressure of the particular ion source above which the ionization efficiency of the source is deleteriously affected. This temperature is $\sim 2.67 \times 10^{-2}$ Pa for the EBPIS used at the HRIBF [13].

Fig. 10. Thermal equilibrium composition of Al_2O_3 as a function of temperature. Note, the limiting temperature of the compound is ~ 2173 K. Fibrous Al_2O_3 target-material has been used to generate useful intensities of $^{17,18}\text{F}$ for astrophysics research at the HRIBF [17,18].

Fig. 11. Thermal equilibrium composition of ZrO_2 as a function of temperature. Note, the compound has a limiting temperature of ~ 2373 K. Fibrous ZrO_2 , in combination with the new concept, kinetic ejection negative ion source [16], has been tested and found to be a viable candidate target-material for the generation of high-intensity $^{17,18}\text{F}$ RIBs for astrophysics research at the HRIBF [17,18].

Fig. 12. Thermal equilibrium composition of HfO_2 as a function of temperature. Note, the compound has a limiting temperature of ~ 2573 K. Fibrous HfO_2 , in combination with the new concept, kinetic ejection negative ion source [16], has been used to generate intensities of $^{17,18}\text{F}$ RIBs for astrophysics research at the HRIBF [19].

Fig. 13. Vapor pressures of UC_2 and ThC_2 . These targets are candidates for the production of a variety of neutron-rich, radio-nuclei and will be operated up to the limiting temperatures set by the vapor pressure of the particular ion source above which the ionization efficiency of the source is deleteriously affected. This temperature is $\sim 2.67 \times 10^{-2}$ Pa for the EBPIs used at the HRIBF [13].

Fig. 14. Thermal equilibrium composition of UC_2 as a function of temperature. UC_2 has been coated onto RVCF to form fission targets for the efficient release of a wide variety of neutron-rich radioactive species for potential use in the nuclear physics research program at the HRIBF [22].

Fig. 15. Thermal equilibrium composition of ThC_2 as a function of temperature. ThC_2 is a candidate fission target-material for the production of neutron-rich radioactive species for potential use in the nuclear physics research program at the HRIBF.

Fig. 16. Simulation of the diffusion release of ^{17}F from ZrO_2 from a planar geometry target of thickness x_p ; from a cylindrical geometry target of diameter d_c ; and from a spherical geometry target of diameter d_s where $x_p = d_c = d_s$; D is assumed to have value: $D = 2.2 \times 10^{-14} m^2/s$.

Fig. 17. Scanning Electron Micrograph (SEM) of Rh ($\rho \sim 8\% \rho_0$) metal foam for potential use a spallation target for high-energy ISOL facilities or for wicking liquid-metal target-materials into the paths of horizontally impinging production beams.

Fig. 18. Scanning Electron Micrograph (SEM) of SiO_2 fibrous material for use in producing S and P RIBs.

Fig. 19. Scanning Electron Micrograph (SEM) of HfO_2 fibrous material used to produce and efficiently release $^{17,18}F$ at the HRIBF [19].

Fig. 20. Scanning Electron Micrograph (SEM) of a carbon-bonded-carbon fiber (CBCF) matrix (fiber diameter: $6 \mu m$) coated by chemical vapor infiltration (CVI) with $5 \mu m$ of SiC . The composite target matrix is highly permeable and will be tested for the release of short-lived P and S isotopes.

Fig. 21. Scanning Electron Micrograph (SEM) of reticulated-vitreous-carbon-fiber (RVCF) matrix electroplated with $\sim 3 \mu m$ Ni for potential use in generating ^{58}Cu .

Fig. 22. Scanning Electron Micrograph (SEM) of reticulated-vitreous-carbon-fiber (RVCF) matrix CVD coated with W .

Fig. 23. Scanning Electron Micrograph (SEM) of reticulated-vitreous-carbon-fiber (RVCF) matrix coated by sequential chemical reactions to form $\sim 14 \mu m$ ($\sim 1 g/cm^3$) of UC_2 . The composite target matrix is highly permeable and efficiently releases a variety of short-lived, neutron-rich radioactive species [22].

Fig. 24. Liquid-metal target scenario for potential use in generating ^{58}Cu /liquid- Ni or ^{69}As /liquid- Ge at the HRIBF. The thickness of the liquid layer is chosen to diffusively-release the particular specie within its lifetime while the impingement angle for the production beam is chosen to optimize the interaction length so that the species of interest is optimally produced.

Fig. 25. Target/heat-sink scenario for removing heat from Al_2O_3 fibrous target-material for potential use in generating $^{17,18}F$ for the HRIBF astrophysics research program.

Table 1. Candidate Targets for RIB Generation at the HRIBF

Beam	$\tau_{1/2}$	Reaction	Target Materials	Limiting Temp. (°C)	Release Product
^{13}N	9.97 m	$^{12}\text{C}(\text{d},\text{n})^{13}\text{N}$	C	2398	CN
^{14}O	70 s	$^{12}\text{C}(\text{}^3\text{He},\text{n})^{14}\text{O}$	C	2398	CO
^{14}O	70 s	$^{14}\text{N}(\text{p},\text{n})^{14}\text{O}$	BN	1893	BO
^{15}O	2.0 m	$^{12}\text{C}(\text{}^4\text{He},\text{n})^{15}\text{O}$	C	2298	CO
^{15}O	2.0 m	$^{14}\text{N}(\text{d},\text{n})^{15}\text{O}$	BN	1983	BO
^{10}C	19 s	$^{10}\text{B}(\text{p},\text{n})^{10}\text{C}$	BN	1893	CN
^{10}C	19 s	$^9\text{Be}(\text{}^3\text{He},2\text{n})^{10}\text{C}$	BeO	2473	CO
^{11}C	20 m	$^{11}\text{B}(\text{p},\text{n})^{11}\text{C}$	BN	1893	CN
^{11}C	20 m	$^9\text{Be}(\text{}^4\text{He},2\text{n})^{11}\text{C}$	BeO	2473	CO
^{17}F	64 s	$^{16}\text{O}(\text{d},\text{n})^{17}\text{F}$	$\text{Al}_2\text{O}_3, \text{ZrO}_2, \text{HfO}_2$	2178,2373,2573	F_x, AlF
^{18}F	1.8 h	$^{17}\text{O}(\text{d},\text{n})^{18}\text{F}$	$\text{Al}_2\text{O}_3, \text{ZrO}_2, \text{HfO}_2$	2173,2373,2573	F_x, AlF
^{18}F	1.8 h	$^{16}\text{O}(\alpha, \text{pn})^{18}\text{F}$	$\text{Al}_2\text{O}_3, \text{ZrO}_2, \text{HfO}_2$	2178,2373,2573	F_x, AlF
^{17}F	6.4 s	$^{14}\text{N}(\text{}^4\text{He},\text{n})^{17}\text{F}$	BN	1893	BF
^{18}F	1.8 h	$^{15}\text{N}(\text{}^4\text{He},\text{n})^{18}\text{F}$	BN	1893	BF
^{21}Na	22.5 s	$^{24}\text{Mg}(\text{p},\alpha)^{21}\text{Na}$	MgO	1803	Na,NaO
^{25}Al	7.17 s	$^{28}\text{Si}(\text{}^3\text{He},\alpha\text{pn})^{25}\text{Al}$	Zr_5Si_3	2273	Al
^{29}P	4.1 s	$^{28}\text{Si}(\text{d},\text{n})^{29}\text{P}$	SiC, SiO ₂	1933,1773	$\text{P}, \text{P}_x\text{O}_y$
^{29}P	4.1 s	$^{27}\text{Al}(\text{}^3\text{He},\text{n})^{29}\text{P}$	$\text{AlB}_2, \text{AlPO}_4$	1923,1853	$\text{P}, \text{P}_x\text{O}_y$
^{30}P	2.5 m	$^{30}\text{Si}(\text{p},\text{n})^{30}\text{P}$	SiC, SiO ₂	1933,1773	$\text{P}, \text{P}_x\text{O}_y$
^{30}P	2.5 m	$^{27}\text{Al}(\text{}^4\text{He},\text{n})^{30}\text{P}$	$\text{AlB}_2, \text{AlPO}_4$	1923,1853	$\text{P}, \text{P}_x\text{O}_y$
^{30}S	1.2 s	$^{28}\text{Si}(\text{}^3\text{He},\text{n})^{30}\text{S}$	SiO ₂	1773	S,SO ₂
^{30}S	1.2 s	$^{28}\text{Si}(\text{}^4\text{He},2\text{n})^{30}\text{S}$	SiO ₂	1773	S,SO ₂
^{30}S	1.2 s	$^{28}\text{Si}(\text{}^3\text{He},\text{n})^{30}\text{S}$	SiC	1933	CS
^{30}S	1.2 s	$^{28}\text{Si}(\text{}^4\text{He},2\text{n})^{30}\text{S}$	SiC	1933	CS
^{31}S	2.9 s	$^{28}\text{Si}(\text{}^4\text{He},\text{n})^{31}\text{S}$	SiO ₂	1773	S,SO
^{31}S	2.9 s	$^{28}\text{Si}(\text{}^4\text{He},\text{n})^{31}\text{S}$	SiC	1873	CS

Table 1. Candidate Targets for RIB Generation at the HRIBF (continued)

Beam	$\tau_{1/2}$	Reaction	Target Materials	Limiting Temp. (°C)	Release Product
^{33}Cl	2.5 s	$^{32}\text{S}(\text{d},\text{n})^{33}\text{Cl}$	CaS,LaS,CeS	1773,1948,2033	CaCl,CeCl,LaCl
^{34}Cl	32 m	$^{34}\text{S}(\text{p},\text{n})^{34}\text{Cl}$	CaS,LaS,CeS	1773,1948,2033	CaCl,CeCl,LaCl
^{36}K	0.34 s	$^{40}\text{Ca}(\text{p},\alpha\text{n})^{36}\text{K}$	CaO	1973	K,KO
^{37}K	1.3 s	$^{40}\text{Ca}(\text{p},\alpha)^{37}\text{K}$	CaO	1973	K,KO
^{38}K	7.5 m	$^{40}\text{Ca}(\text{d},\alpha)^{38}\text{K}$	CaO	1973	K,KO
^{52}Fe	8.28 h	$^{52}\text{Cr}(\text{}^3\text{He},3\text{n})^{52}\text{Fe}$	$\text{Cr}_2\text{O}_3,\text{MnC}_2$	2123,2923	$\text{FeO},\text{Fe}_2\text{O}_3,\text{Fe}$
^{52}Fe	8.28 h	$^{50}\text{Cr}(\text{}^3\text{He},\text{n})^{52}\text{Fe}$	$\text{Cr}_2\text{O}_3,\text{MnC}_2$	2123,2923	$\text{FeO},\text{Fe}_2\text{O}_3,\text{Fe}$
^{55}Fe	2.73Y	$^{55}\text{Mn}(\text{p},\text{n})^{55}\text{Fe}$	MnC_2	2923	Fe
^{58}Cu	3.25	$^{58}\text{Ni}(\text{p},\text{n})^{58}\text{Cu}$	Ni	1573	Cu
^{63}Ga	31 s	$^{64}\text{Zn}(\text{p},2\text{n})^{63}\text{Ga}$	ZnO	1613	Ga
^{64}Ga	74 s	$^{64}\text{Zn}(\text{p},\text{n})^{64}\text{Ga}$	ZnO	1613	Ga
^{66}Ga	9.5 h	$^{70}\text{Ge}(\text{}^3\text{He},\alpha\text{p}2\text{n})^{66}\text{Ga}$	$\text{Zr}_5\text{Ge}_3,\text{Ge}$	~2273,1433	Ga
^{67}Ga	3.26 d	$^{70}\text{Ge}(\text{p}\alpha)^{67}\text{Ga}$	$\text{Zr}_5\text{Ge}_3,\text{Ge}$	~2273,1433	Ga
^{67}Ga	3.26 d	$^{70}\text{Ge}(\text{}^3\text{He},\alpha\text{pn})^{67}\text{Ga}$	$\text{Zr}_5\text{Ge}_3,\text{Ge}$	~2273,1433	Ga
^{68}Ga	1.1 h	$^{70}\text{Ge}(\text{p},2\text{pn})^{68}\text{Ga}$	$\text{Zr}_5\text{Ge}_3,\text{Ge}$	~2273,1433	Ga
^{63}Ga	31 s	$^{63}\text{Cu}(\text{}^3\text{He},3\text{n})^{63}\text{Ga}$	Cu	1323	Ga
^{64}Ga	64 s	$^{63}\text{Cu}(\text{}^3\text{He},2\text{n})^{64}\text{Ga}$	Cu	1323	Ga
^{69}As	15 m	$^{70}\text{Ge}(\text{p},2\text{n})^{69}\text{As}$	$\text{Zr}_5\text{Ge}_3,\text{Ge}$	~2273,1433	As
^{70}As	63 m	$^{70}\text{Ge}(\text{p},\text{n})^{70}\text{As}$	$\text{Zr}_5\text{Ge}_3,\text{Ge}$	~2223,1433	As
^{71}Se	4.7 m	$^{70}\text{Ge}(\text{}^3\text{He},2\text{n})^{71}\text{Se}$	$\text{Zr}_5\text{Ge}_3,\text{Ge}$	~2223,1433	Se
^{72}Se	8.4 d	$^{70}\text{Ge}(\text{}^4\text{He},2\text{n})^{72}\text{Se}$	$\text{Zr}_5\text{Ge}_3,\text{Ge}$	~2223,1433	Se
^{75}Br	1.62 s	$^{76}\text{Se}(\text{p},2\text{n})^{75}\text{Br}$	LaSe	1933	Br,LaBr
^{76}Br	16 h	$^{76}\text{Se}(\text{p},\text{n})^{76}\text{Br}$	LaSe	1933	Br,LaBr

Table 2. Candidate Spallation and Fission Target Materials for High-Energy (1-GeV) Proton Beam Facilities

Target Material	Limiting Temp °K	Product Species
BeO	2503	He → F
C	2240	He → N
Al ₂ O ₃	1998	He → Si
SiC	1973	He → P
TiC	2323	He → V
Sc ₂ O ₃	2048	He → Ti
VC	2203	He → Cr
MnC ₂	2973	He → Fe
Y ₂ O ₃	2223	He → F; Al → Zr
Zr	2303	P → Nb
ZrC	2648	P → Nb; He → N
ZrO ₂	2323	He → F; Si → Nb
Nb	2353	P → Mo
NbC	2493	He → N; P → Mo
Mo	2263	S → Tc
CeC ₂	2663	He → N; Cu → Nd
CeO ₂	2173	He → O; Cu → Nd
HfO ₂	2473	He → Ta
Ta	2923	He → W
TaC	2613	He → W
W	3136	He → Re
WC	2753	He → Re
Re	2873	He → Os
ThC ₂	2923	He → Pa
UC ₂	2373	He → Np

Table 3. Permissible Target Thicknesses

Species	$\tau_{1/2}$ (s)	Target Material	Temp. ($^{\circ}$ K)	D (cm ² /s)	x (μ m)	d_r (μ m)	d_s (m)
¹⁷ F	64.5	Al ₂ O ₃	1973	1×10^{-10}	2.5	3.8	5
¹⁸ F	6588	Al ₂ O ₃	1973	1×10^{-10}	25	38	50
⁵⁸ Cu	3.2	Ni	1633	3.2×10^{-9}	3.2	4.9	6.4
⁵⁸ Cu	3.2	Ni _{liq}	1633	3×10^{-5}	308	470.3	616
⁶⁹ As	912	Ge _{liq}	1423	5×10^{-5}	6708	10250	13416
¹³² Sn	40	U	1408	4×10^{-8}	40	61	80
¹³² Sn	40	Th _{liq}	1700	1×10^{-5}	628	960	1256
¹³² Sn	40	Th	2028	4×10^{-5}	400	611	800
¹³² Sn	40	Th _{liq}	2273	5×10^{-5}	1404	2145	2808

Selected radioactive species diffused from: Plates of thickness x
Rods of diameter d_r
Spheres of diameter d_s

Table 4. Liquid-Metal Alloys for Potential Use as RIB Targets

Species	$\tau_{1/2}$ (s)	Target	Target Thickness (μ m)	Target Temp. ($^{\circ}$ K)
⁹ Li	0.18	Th/Zr	29.8	>1653
¹¹ Li	0.0087	Th/Zr	2.1	>1623
¹¹ Be	13.8	Th/Zr	261	>1623
¹² Be	0.024	Th/Zr	11	>1623
³¹ Ar	0.015	V/Zr	8.5	>1538
⁴⁶ Ar	8.4	Th/Zr	204	>1623
³⁵ Kr	0.19	V/Zr	31	>1538
⁵⁴ Kr	0.01	Th/Zr	7	>1623
⁵³ Ni	0.05	V/Zr	15.5	>1538
⁷³ Ni	0.9	Th/Zr	66.5	>1623
⁷¹ Kr	0.1	Th/Zr	22	>1623
⁹⁴ Kr	0.21	Th/Zr	32	>1623
¹⁰³ Sn	7	Pt/Th	186	>1510
¹³⁴ Sn	1.04	Th/Zr	71.5	>1623
²¹⁰ Fr	0.05	Th/Zr	15.5	>1623
²³² Fr	5	Th/Zr	157	>1623

*Assumed diffusion coefficient D: 2×10^{-5} /cm²

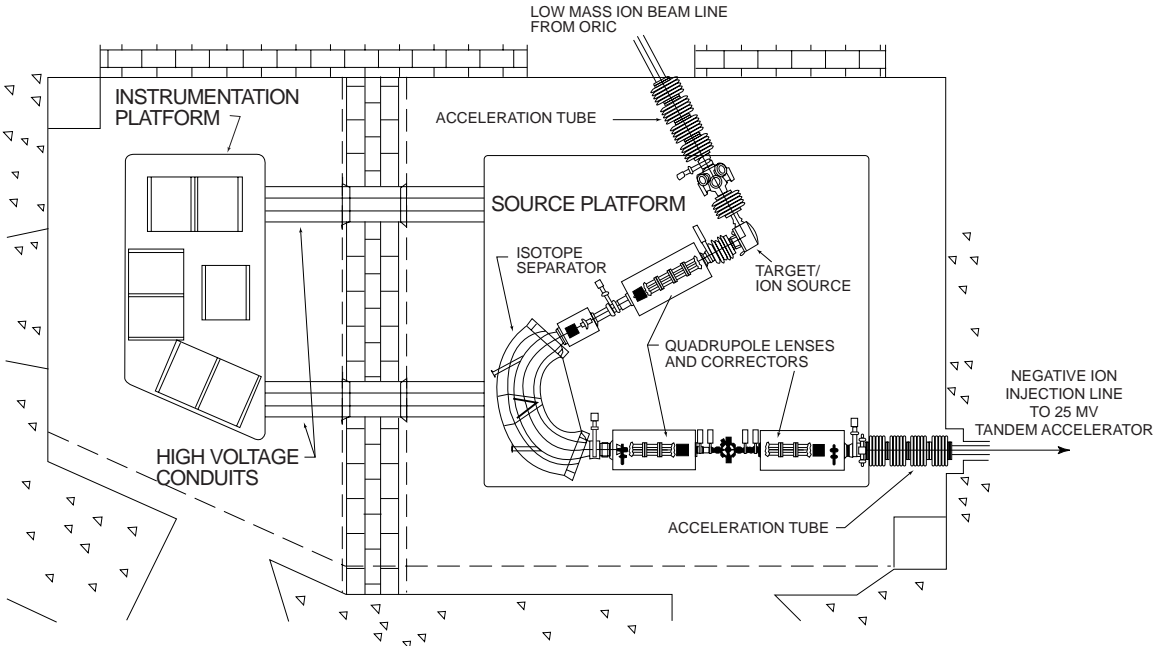


Fig. 1

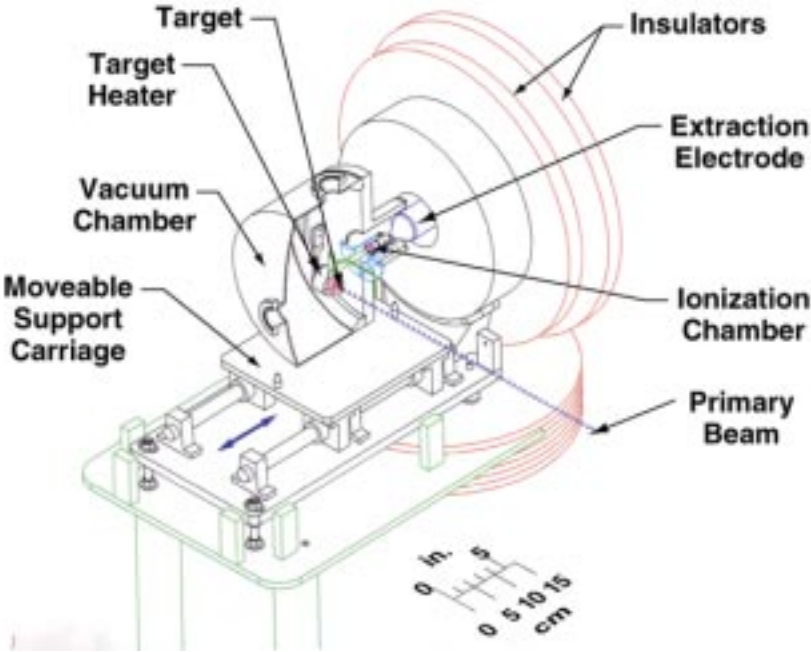


Fig. 2

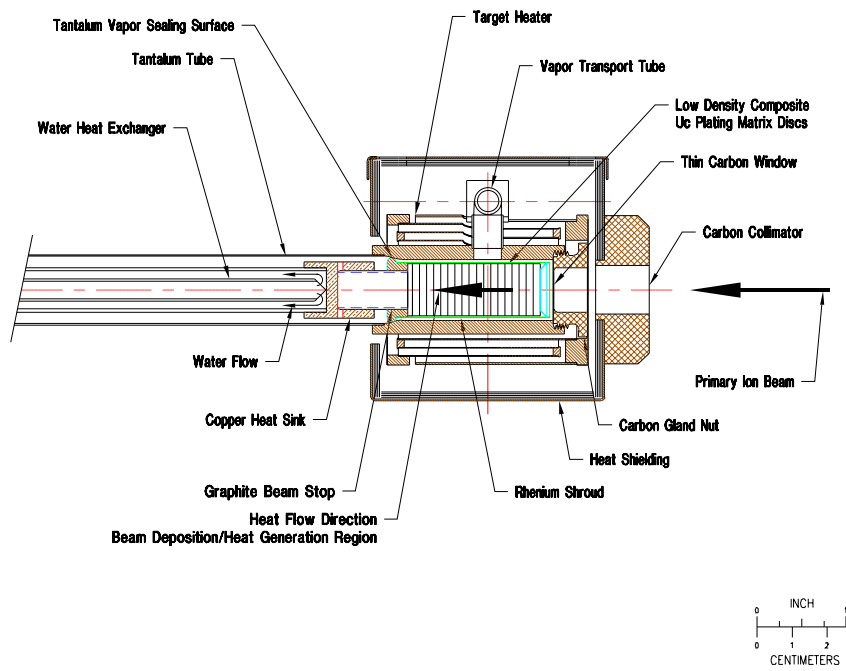


Fig. 3

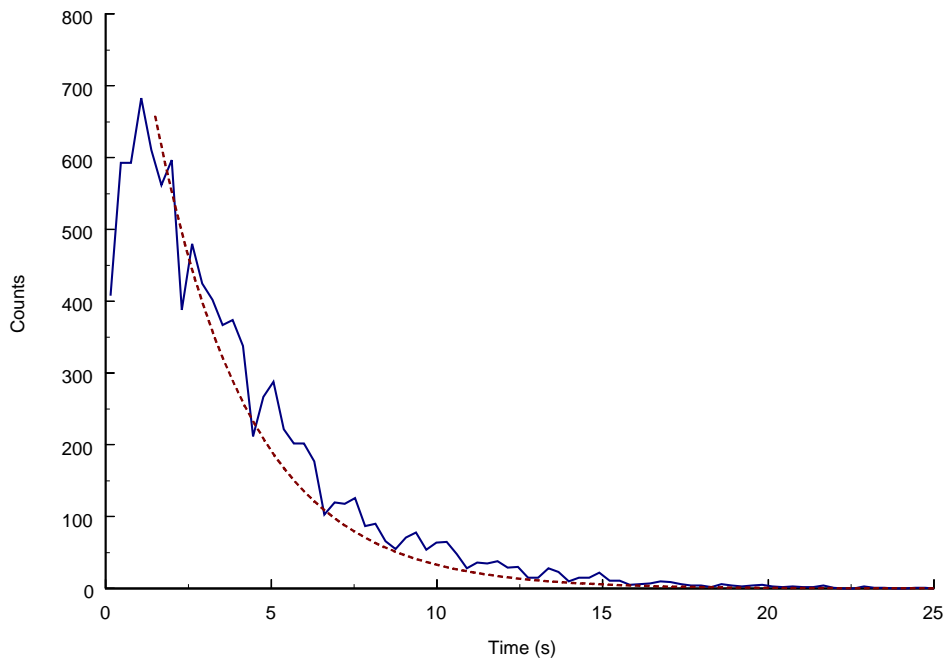


Fig. 4

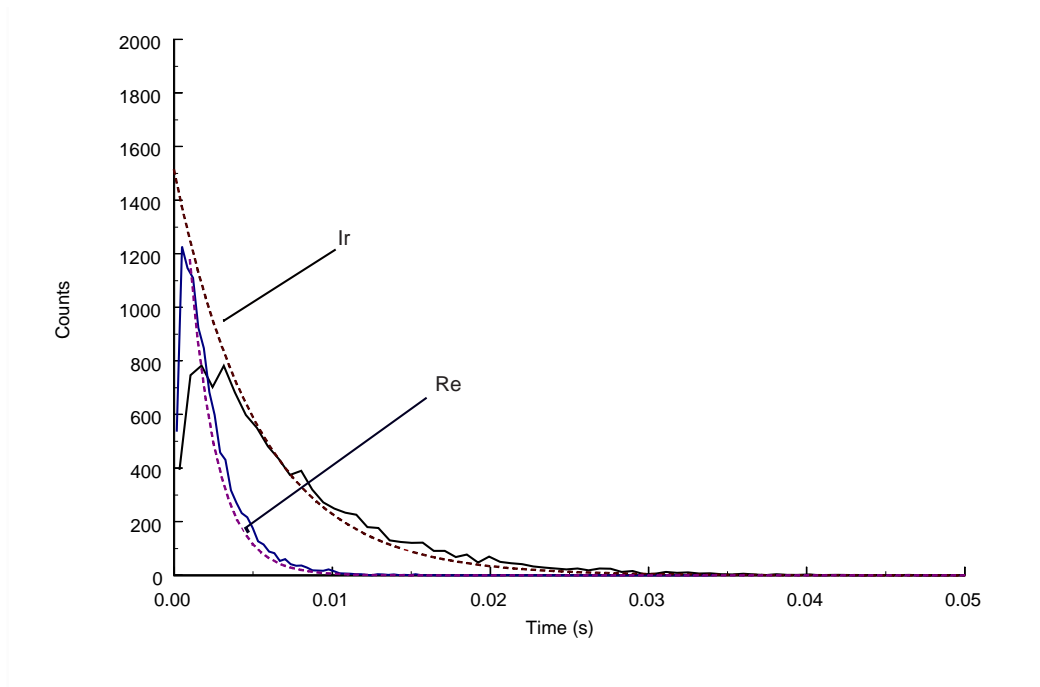


Fig. 5

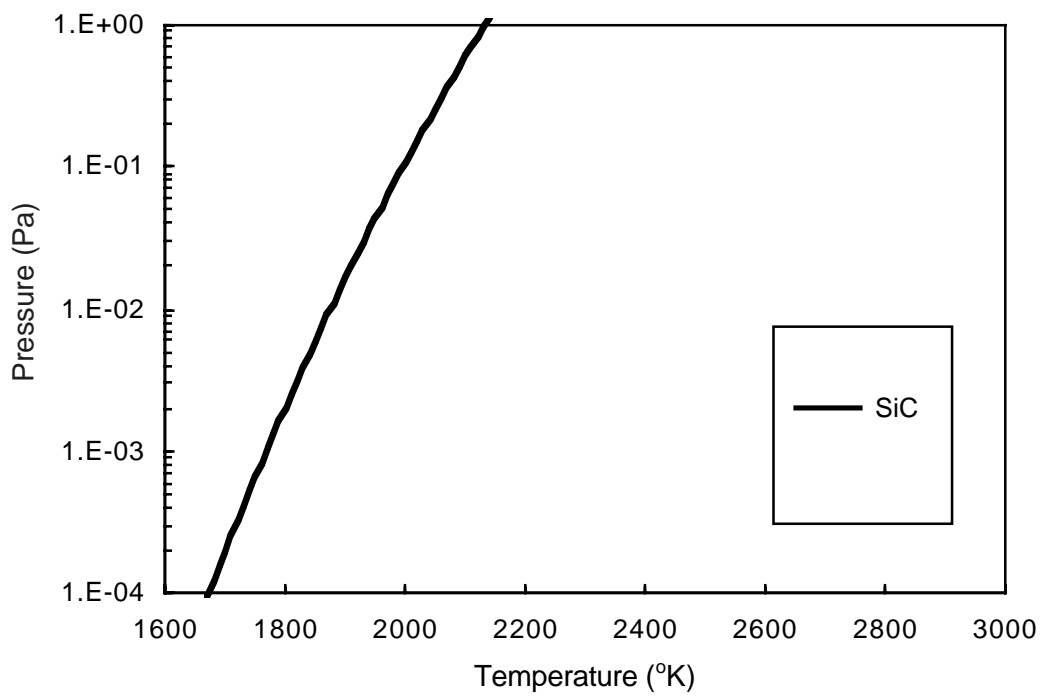


Fig. 6

99-4280A

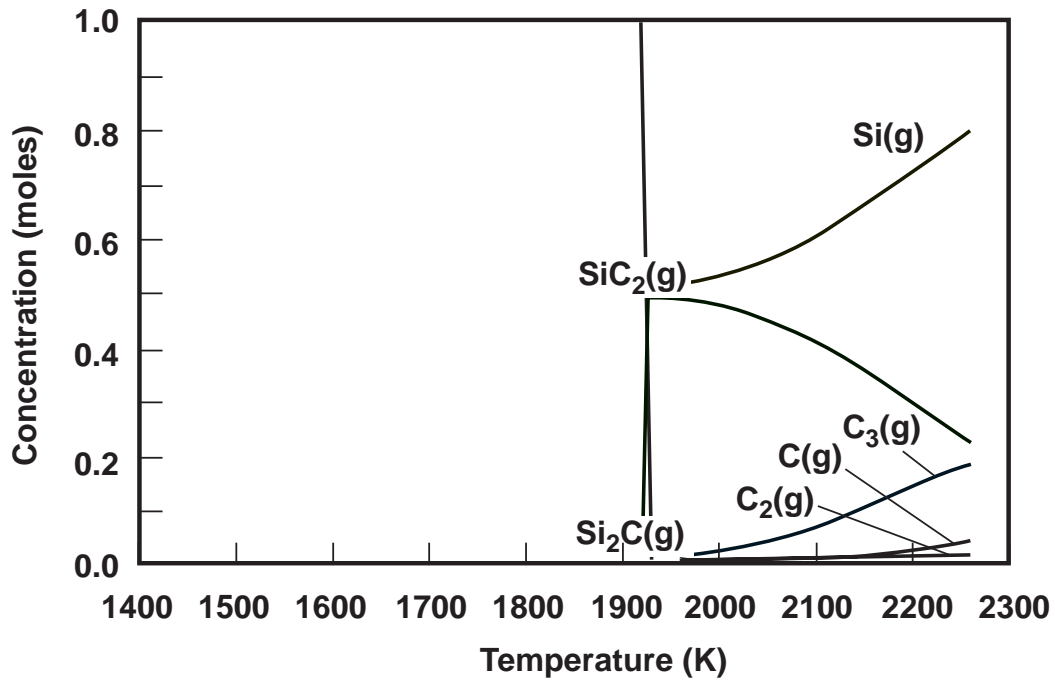


Fig. 7

99-04281A

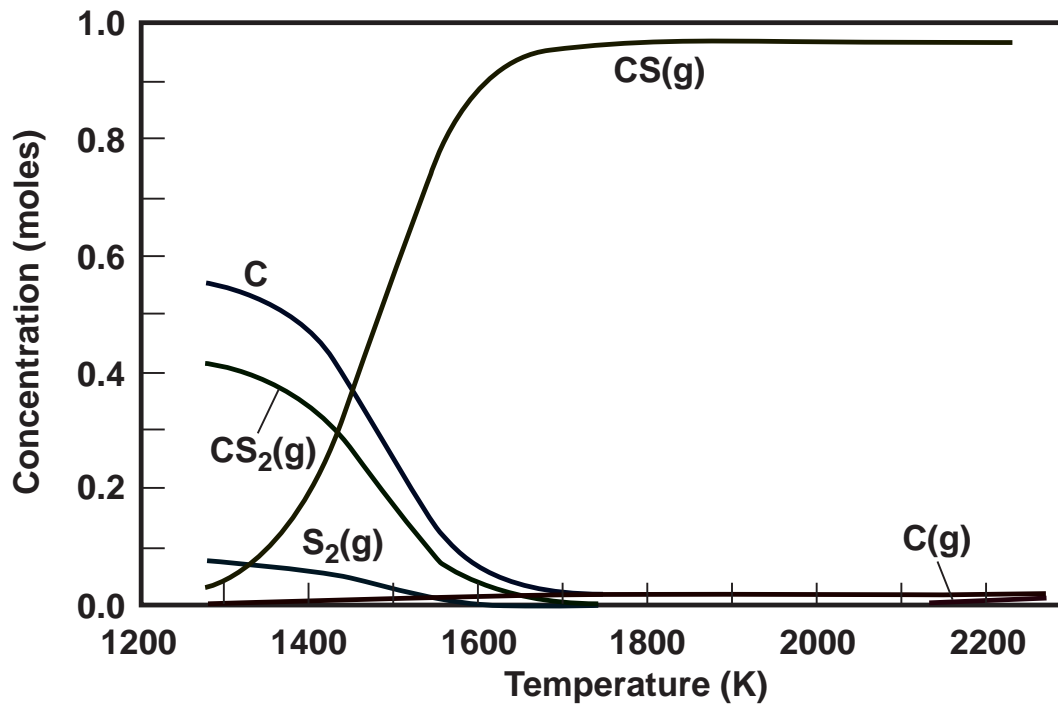


Fig. 8

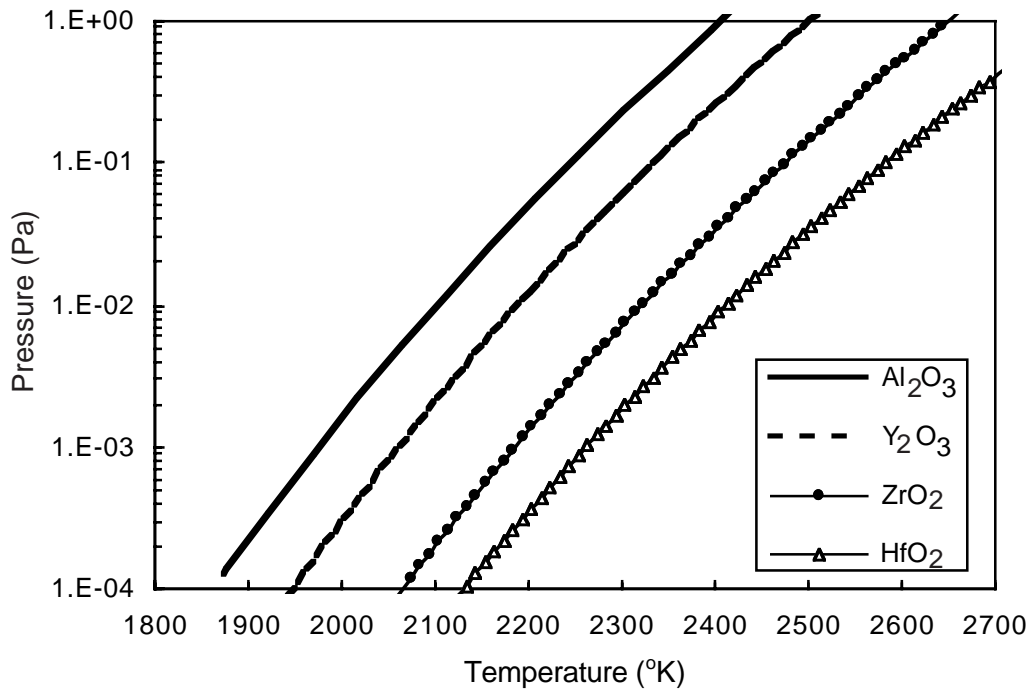


Fig. 9

98-8314A

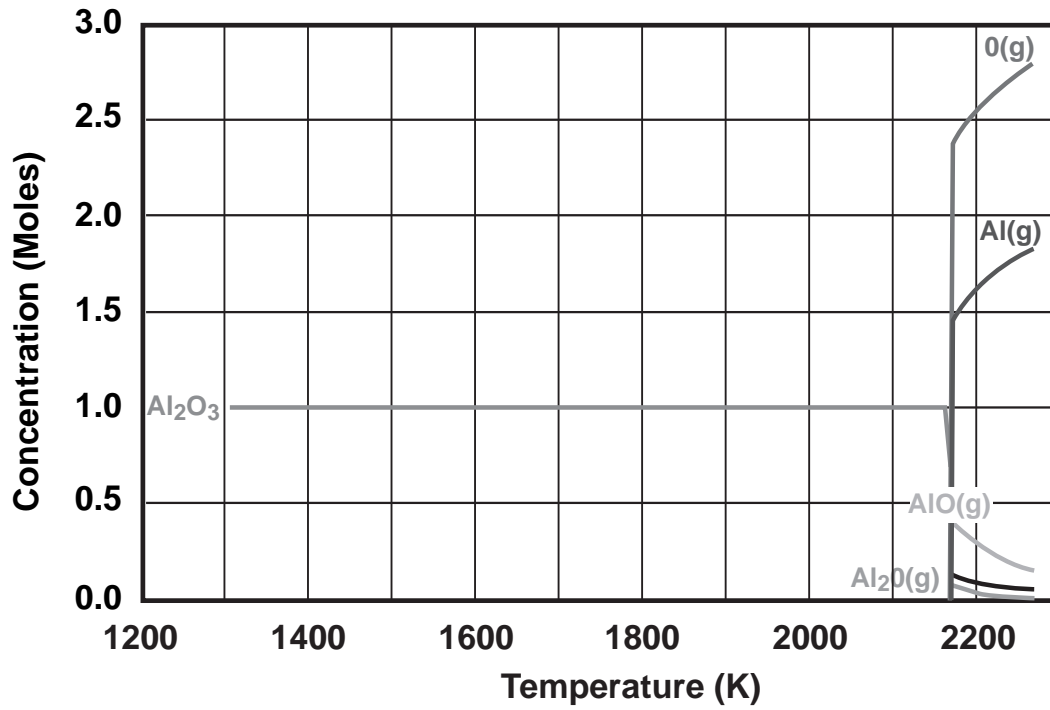


Fig. 10

98-8316A

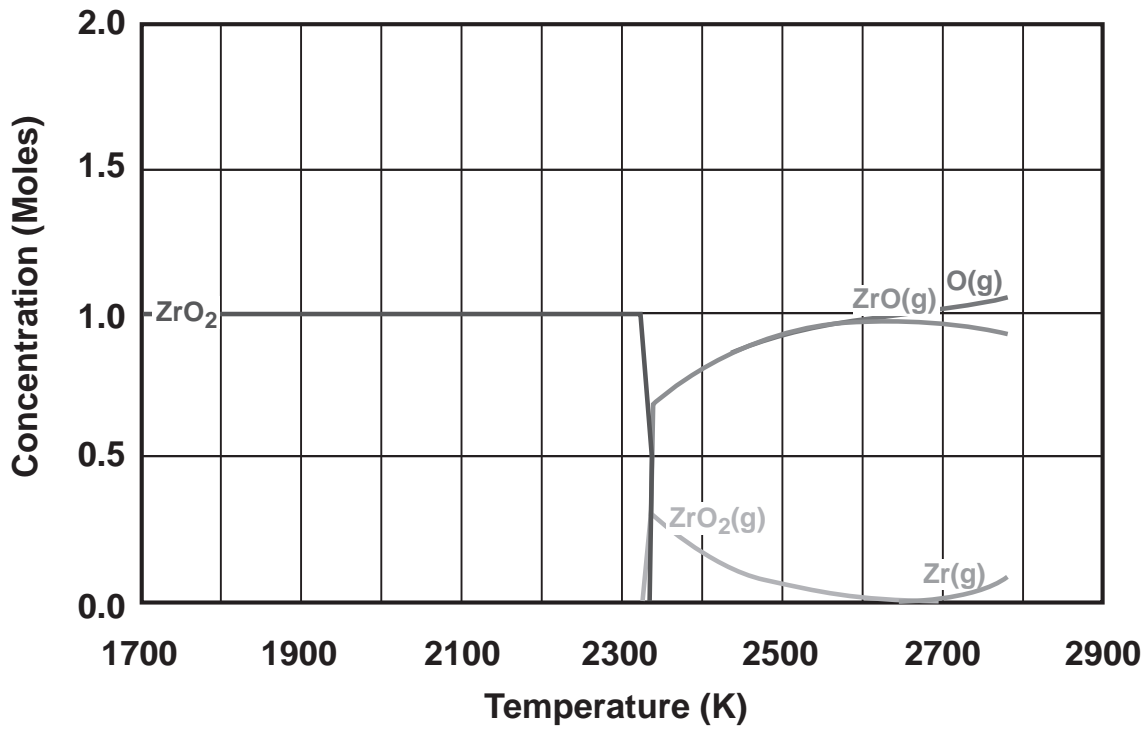


Fig. 11

98-8315A

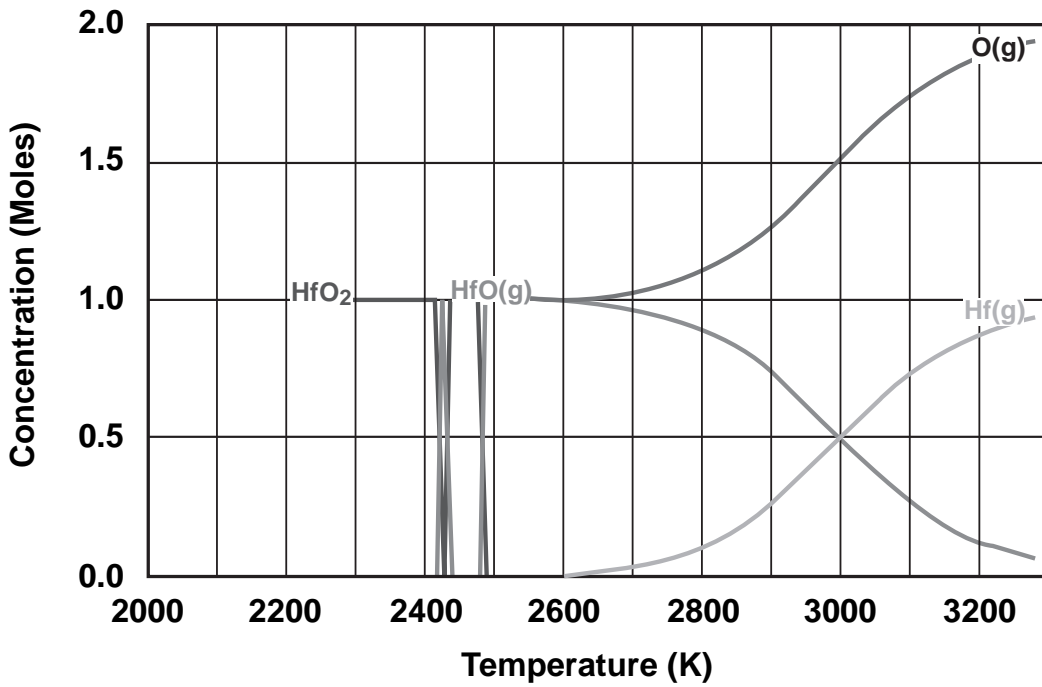


Fig. 12

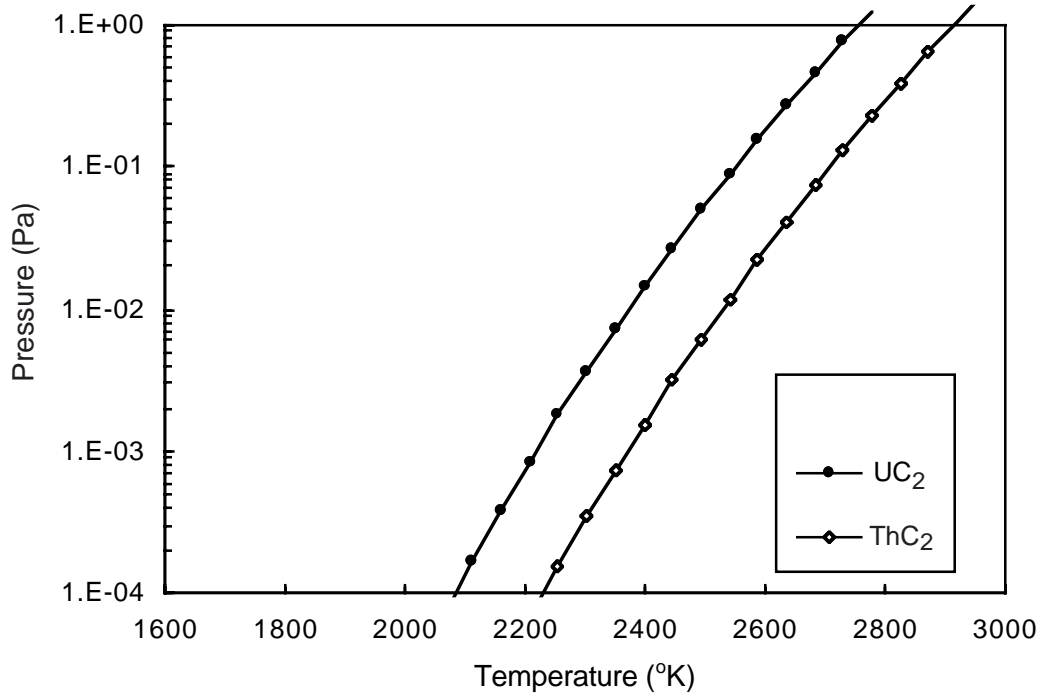


Fig. 13

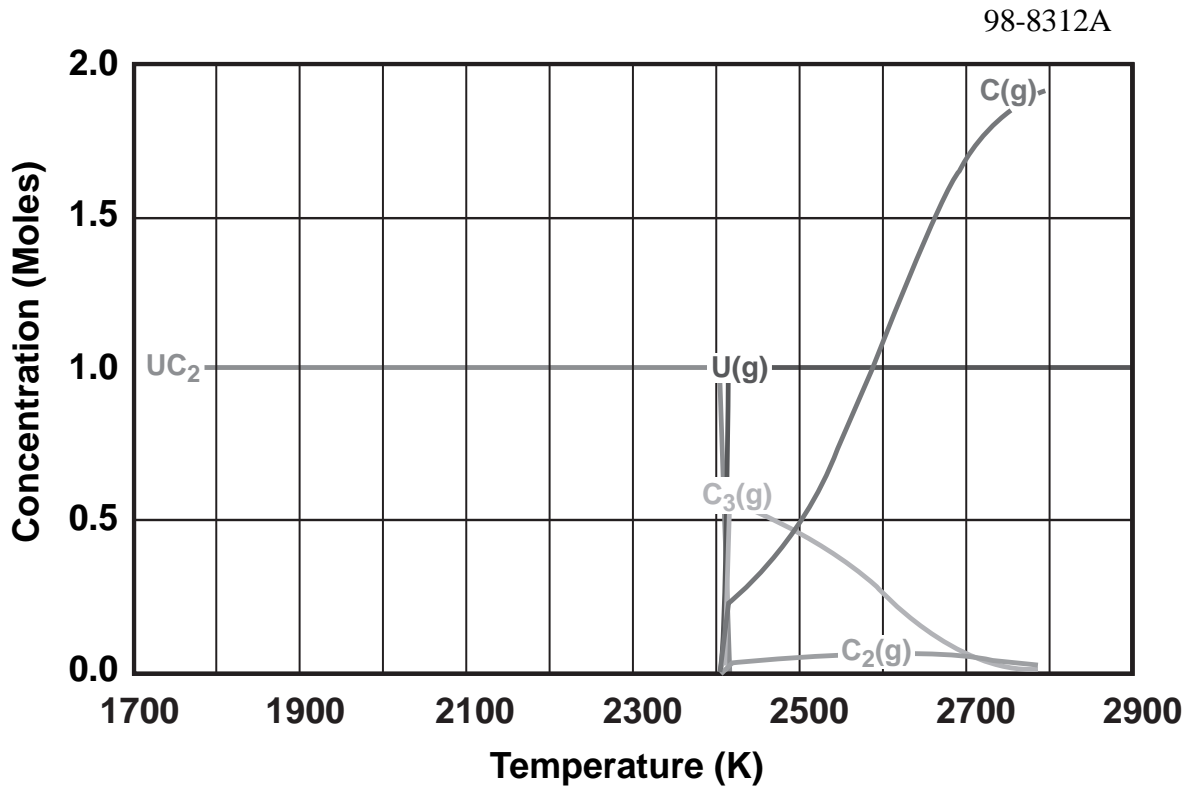


Fig. 14.

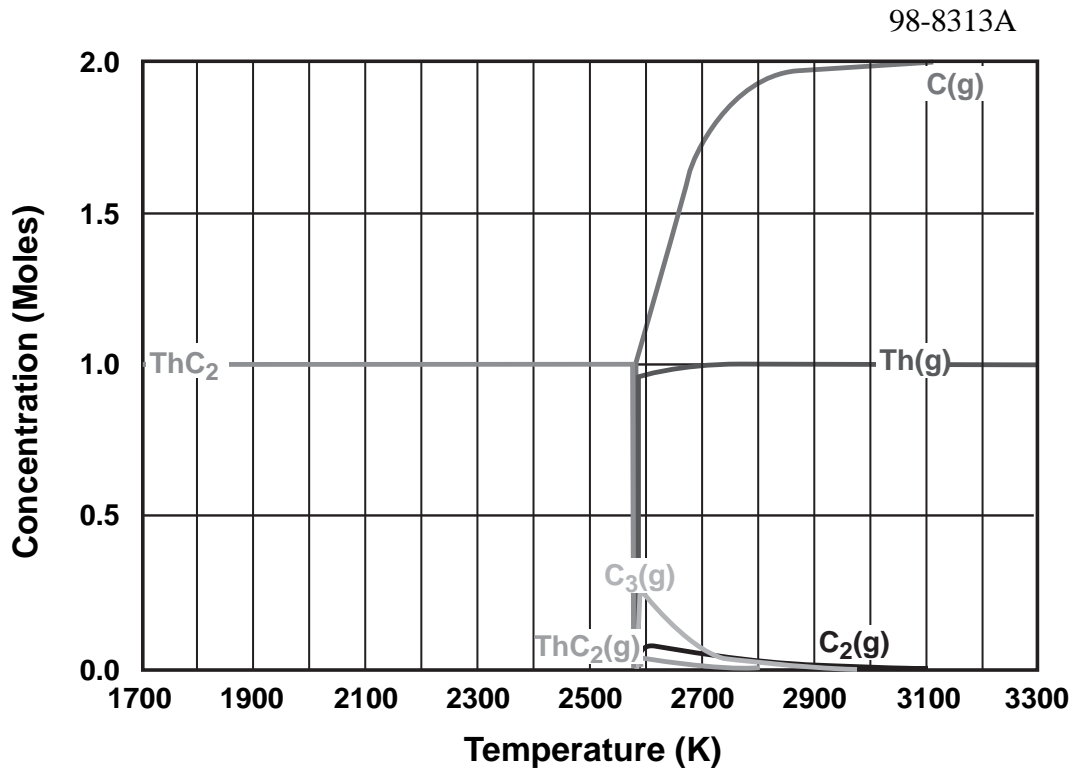


Fig. 15

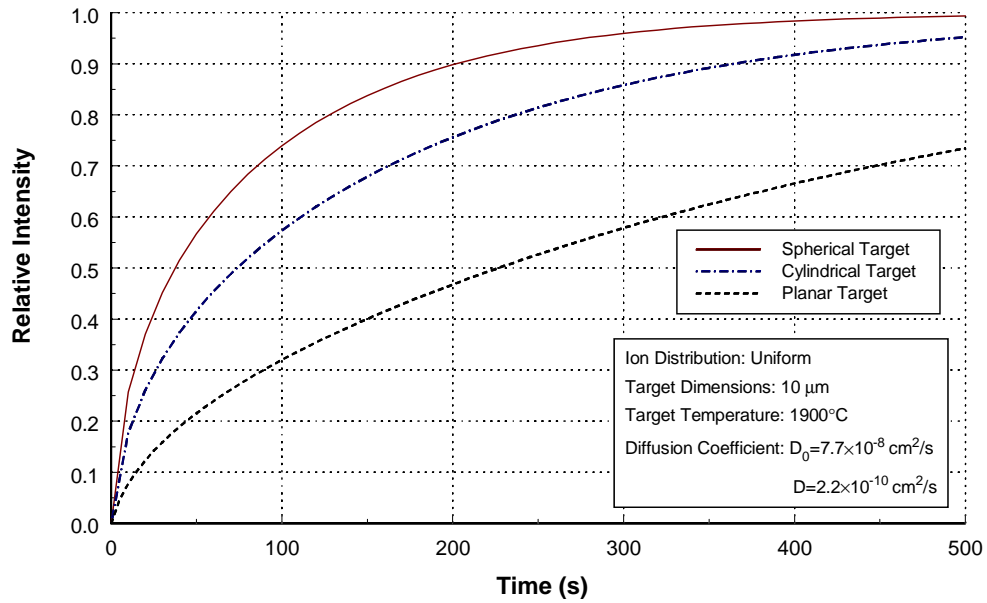
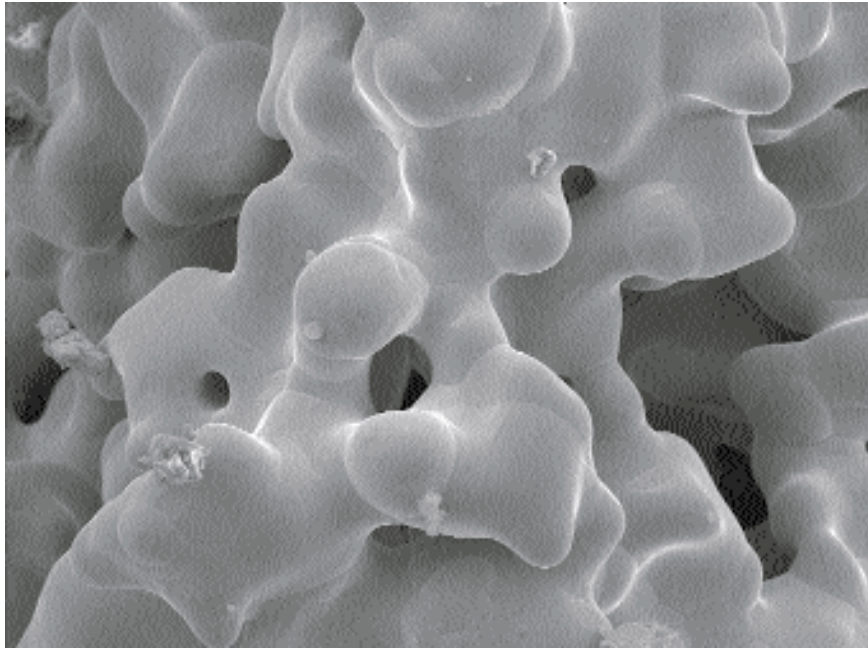
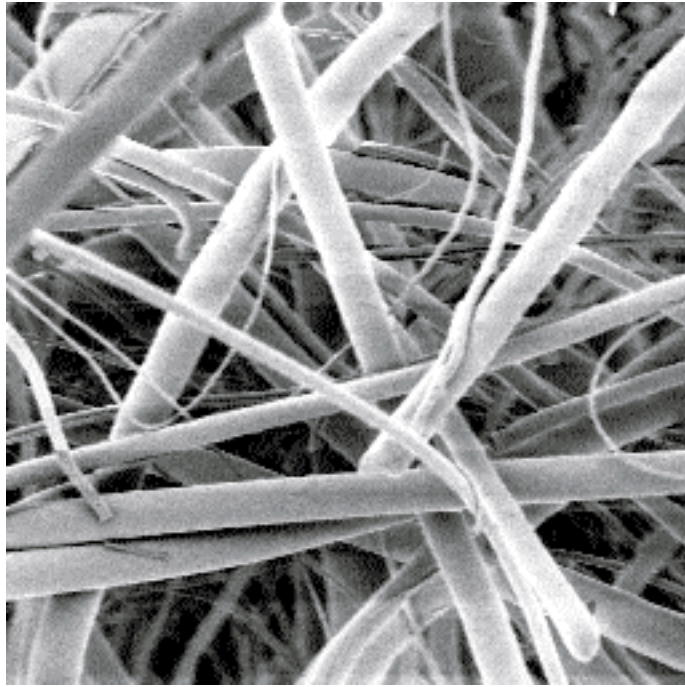


Fig. 16



20 μm

Fig. 17



10 μm

Fig. 18

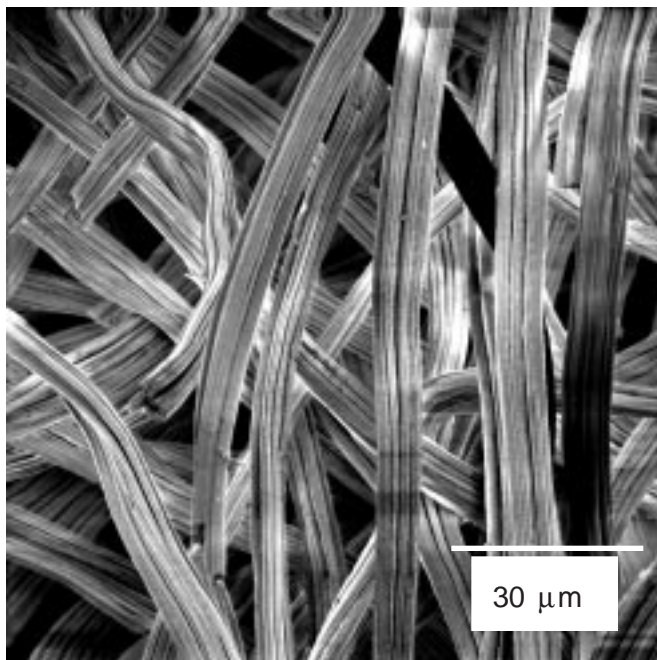


Fig. 19

94M-8758

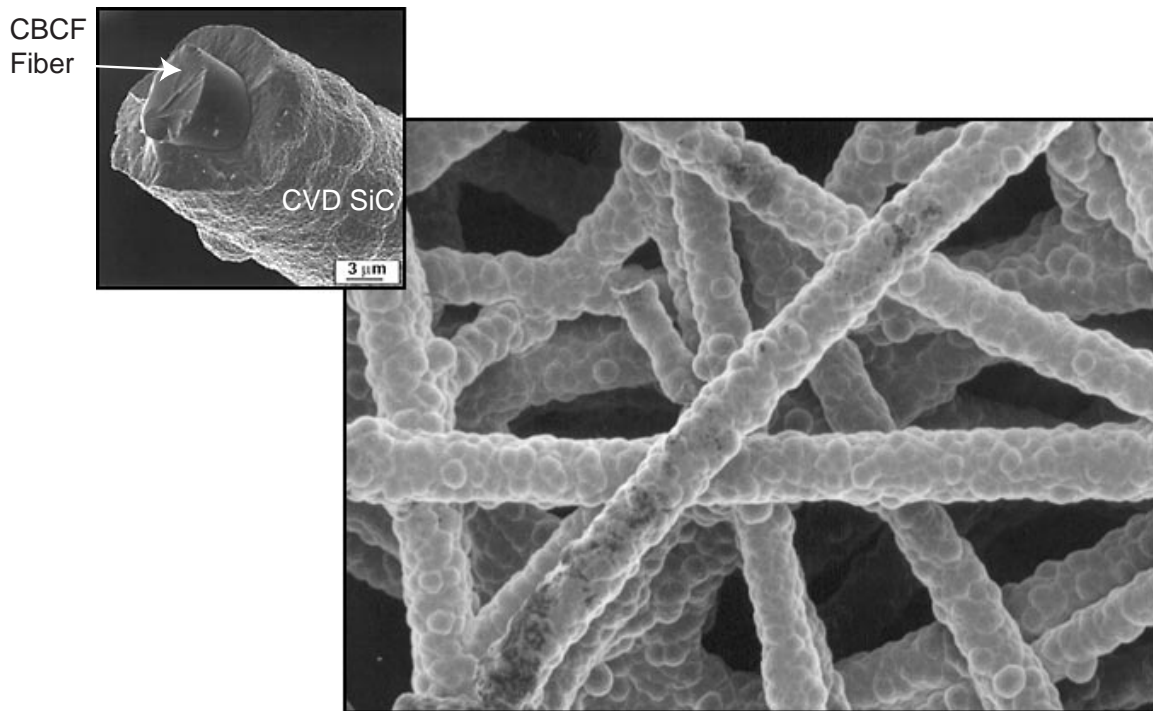


Fig. 20

96M-7518

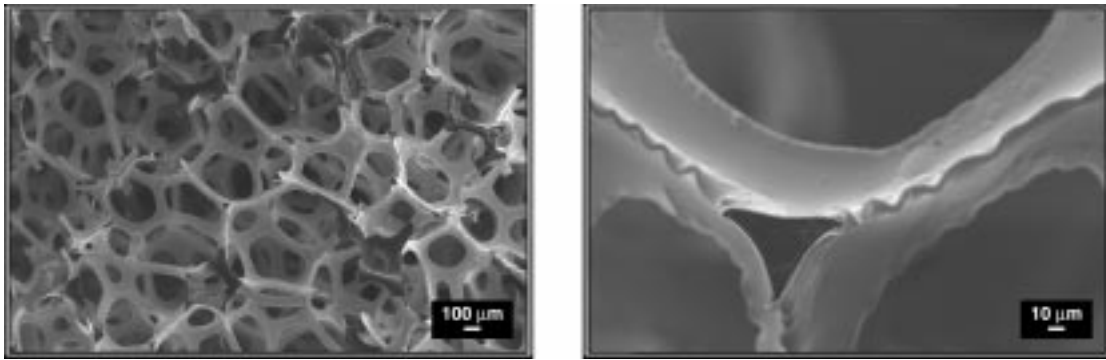


Fig. 21

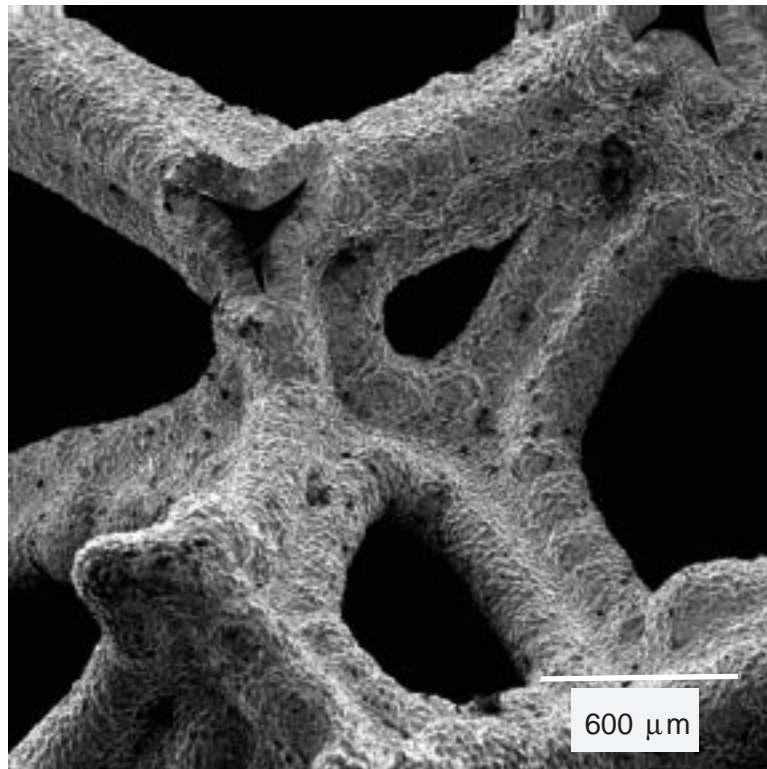


Fig. 22

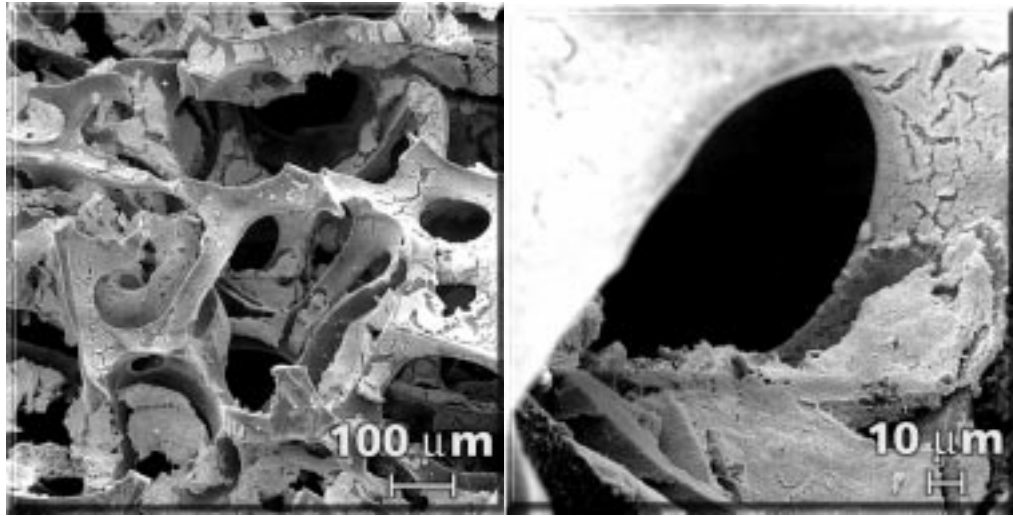


Fig. 23

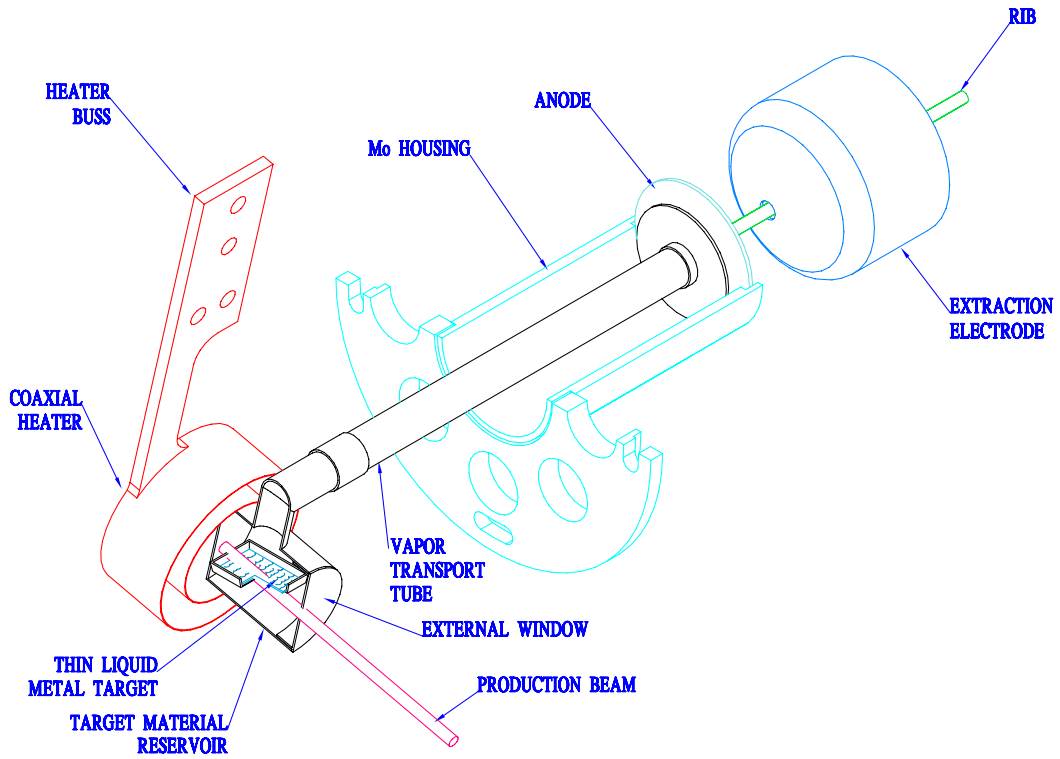


Fig. 24

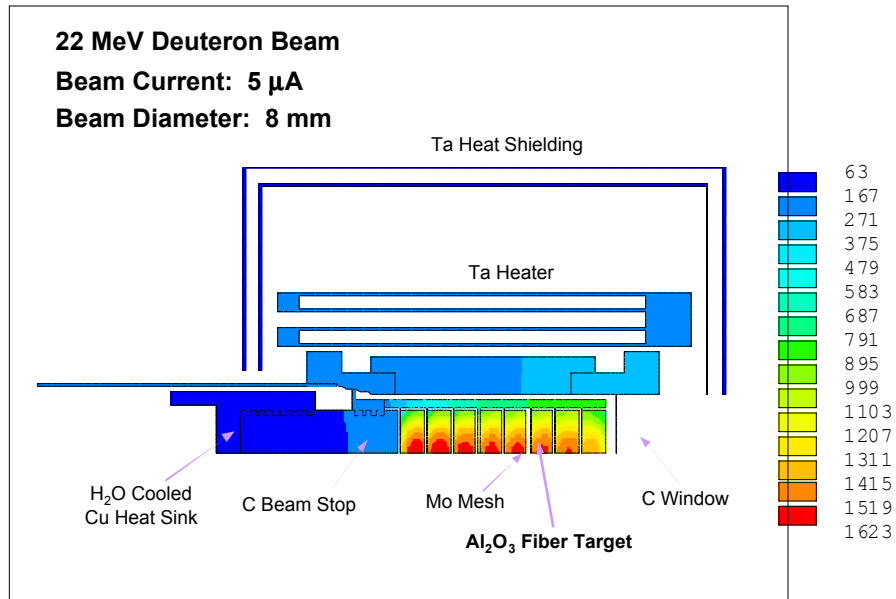


Fig. 25